Modulation of HERG Gating by a Charge Cluster in the N-Terminal Proximal Domain

J. B. Saenen, A. J. Labro, A. Raes, and D. J. Snyders
Laboratory for Molecular Biophysics, Physiology and Pharmacology, Department of Biomedical Sciences, University of Antwerp, Antwerp Belgium

ABSTRACT Human *ether-a-go-go*-related gene (HERG) potassium channels contribute to the repolarization of the cardiac action potential and display unique gating properties with slow activation and fast inactivation kinetics. Deletions in the N-terminal 'proximal' domain (residues 135–366) have been shown to induce hyperpolarizing shifts in the voltage dependence of activation, suggesting that it modulates activation. However, we did not observe a hyperpolarizing shift with a subtotal deletion designed to preserve the local charge distribution, and other deletions narrowed the region to the KIKER containing sequence 362–372. Replacing the positively charged residues of this sequence by negative ones (EIEEE) resulted in a −45 mV shift of the voltage dependence of activation. The shifts were intermediate for individual charge reversals, whereas E365R resulted in a positive shift. Furthermore, the shifts in the voltage dependence were strongly correlated with the net charge of the KIKER region. The apparent speeding of the activation was attributable to the shifted voltage dependence of activation. Additionally, the introduction of negative charges accelerated the intermediate voltage-independent forward rate constant. We propose that the modulatory effects of the proximal domain on HERG gating are largely electrostatic, localized to the charged KIKER sequence.

INTRODUCTION

Voltage-gated potassium channels have been implicated in a variety of physiological processes. The human-*ether-a-go-go*-related gene (HERG or *KCNH2*) encodes potassium channels that contribute to the repolarization of the cardiac action potential. HERG channels display unique gating properties with slow activation kinetics and a fast (C-type) inactivation process. As a result, the channels spend only limited time in the open state upon depolarization (1). Conversely, upon repolarization the rate of recovery from the inactivated state into the open state is much higher than the rate of deactivation (closure). This leads to a large and transient increase of the open probability giving rise to the typical HERG tail current, followed by a slow current decay induced by the progressive closure of the channels (2,3). Impairment of the normal function of HERG can lead to long QT syndrome, a condition which predisposes to ventricular arrhythmia and sudden death (4–6).

The structure of HERG channels is presumably similar to that of other voltage-gated potassium channels: a tetramer of 4 α-subunits composed of six transmembrane segments (S1–S6), a pore loop (P-loop) and the intracellular amino (N) and carboxyl (C) termini (7–9). The S1–S4 transmembrane segments form the voltage-sensing domain that undergoes conformational changes upon perturbation of the transmembrane potential. The main determinant for the voltage sensitivity is an array of positively charged residues located within the S4 segment (10). The cytoplasmic activation gate is located at the bottom part of S6 and allows opening and closure of the permeation pathway (11–13). The N-terminus is composed of a conserved *eag* or PAS (Per-Arnt-Sim) domain (14,15) and a long stretch of ~240 amino acids that has been described as a 'proximal' or 'HERG-specific' domain (Fig. 1) (16).

The PAS domain serves an important role in trafficking of HERG channels to the cell membrane since several mutations in this domain impair the normal trafficking process (17,18). This is further underscored by the amino terminal splice variant HERG 1b that lacks the PAS domain (Fig. 1) (19) and displays only marginal trafficking (20,21). Functionally, the PAS domain has been shown to modulate the deactivation process (14,22,23). From this perspective the first 16 amino acids of the N-terminus have also been implicated in slowing the deactivation process, stabilizing the open state (24–26).

In contrast to the PAS domain, much less is known about the functional role of the proximal domain. Viloria et al. (16) have shown that a series of deletion mutants in this domain resulted in hyperpolarizing shifts of the midpoint of activation that were dependent on the size of the deletion. It was suggested that the entire proximal domain is involved in the modulation of the gating process, although nearly half of the observed effect could be obtained by deletion of only 19 amino acids at the end of this domain. In addition, Gomez-Varela et al. (27) reported that deletion of the proximal domain accelerated the forward rate constants during channel opening.

Here, we report that a short cluster of mainly basic residues, which is located in this 19 residue region proximal to the S1 segment, plays a major role in the N-terminal modulation of HERG activation. We propose that the local electric field of this cluster modulates the activation, likely through

Submitted April 19, 2006, and accepted for publication August 30, 2006.

Address reprint requests to Dirk J. Snyders, MD, PhD, Dept. of Biomedical Sciences, University of Antwerp, Universiteitsplein 1, 2610 Antwerp, Belgium. Tel.: 32-3-820-23-35; Fax: 32-3-820-23-26; E-mail: Dirk.Snyders@ua.ac.be.

0006-3495/06/12/4381/11 $2.00

doi: 10.1529/biophysj.106.087247

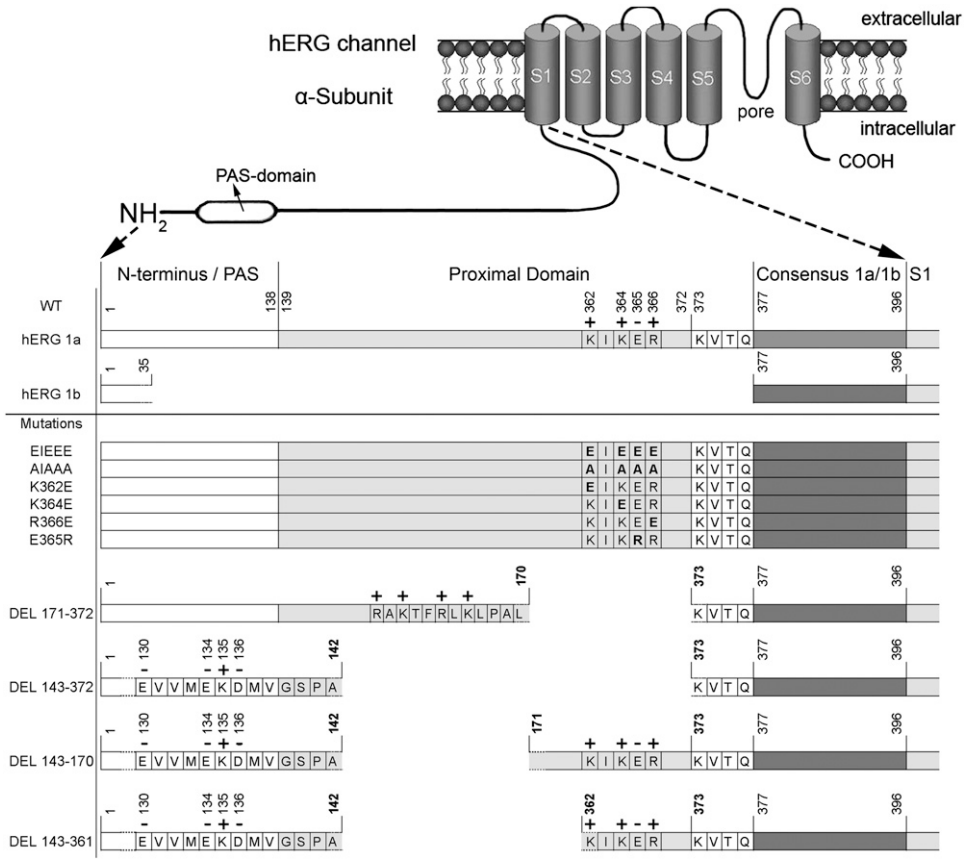

FIGURE 1 Overview of the topology of the HERG N-terminus and the different mutations analyzed. Schematic side view of a HERG α-subunit with six transmembrane segments and a pore loop between S5 and S6, with a detail of the N-terminal sequence underneath (*gray bars* are not to scale). In HERG 1a the sequence of the N-terminus and PAS domain ranges from residues 2 to 138 followed by the proximal or HERG-specific domain that extends from position 139 to 377. The KIKER sequence is part of the 19 terminal amino acids of the proximal domain and starts at position 362 (charged residues are marked on top with ''+'' or ''−'' signs). The common region with HERG 1b starts at residue 377. The HERG 1b splice variant has a short N-terminus, lacking both the PAS and proximal domain; an alternate sequence of 35 residues precedes the common region with HERG 1a. The bottom part shows the different mutations or deletions. The map of the deletions shows the remaining sequence which precedes the deletion.

electrostatic interaction with residues that are located near the channel core.

MATERIALS AND METHODS

Molecular biology

HERG was expressed using the pcDNA3 expression vector. Mutations were introduced by the QuikChange Site-Directed Mutagenesis Kit (Stratagene, La Jolla, CA). After the polymerase chain reaction based mutagenesis, double-stranded sequencing of the channel construct confirmed the presence of the desired modification and the absence of unwanted mutations. Plasmid DNA for mammalian expression was obtained by amplification in XL2 blue-script cells (Stratagene). The plasmid DNA was isolated from the bacterial cells with the NucleoBond AX maxiprep kit (Macherey-Nagel, Düren, Germany) and afterwards the cDNA concentration and purity were determined with ultraviolet absorption.

Electrophysiology

HEK293 cells were cultured in Modified Eagle's Medium supplemented with 10% fetal bovine serum, 1% penicillin/streptomycin, and 1% nonessential amino acids. The cells were transfected with 1.25 μg of wild-type (WT) or mutant subunits cDNA and 0.5 μg eGFP cDNA, using Hekfectin (Bio-Rad, Hercules, CA); and 12–24 h after transfection, the cells were trypsinized and used for analysis within 12 h. Cells were kept in culture at 37°C under a 5% CO_2 atmosphere.

Current recordings were made with an Axopatch-200B amplifier (Axon Instruments, Foster City, CA) in the whole cell configuration of the patch-clamp technique. Experiments were performed at room temperature (20–23°C); current recordings were low pass filtered and sampled at 1–10 kHz with a digidata 1200A data acquisition system (Axon Instruments). Command voltages and data storage were controlled with pCLAMP8 software (Axon Instruments). Patch pipettes were pulled from 1.2-mm Kwik-Fil Borosilicate Glass Capillaries (World Precision Instruments, Sarasota, FL) with a P-2000 puller (Sutter Instruments, Novato, CA). After heat polishing, the resistance of the patch-pipettes was <3 MΩ in the standard extracellular solution containing (in mM) NaCl 130, KCl 4, $CaCl_2$ 1.8, $MgCl_2$ 1, HEPES 10, Glucose 10, adjusted to pH 7.35 with NaOH. The pipettes were filled with intracellular solution containing (in mM) KCl 110, K_4BAPTA 5, K_2ATP 5, $MgCl_2$ 1, HEPES 10, and adjusted to pH 7.2 using KOH. Junction potentials were zeroed with the filled pipette in the bath solution. The remaining liquid junction potential was not corrected and was calculated to be 1.7 mV. After achieving a gigaohm seal, the whole cell configuration was obtained by suction. Capacitive transients were elicited by applying a -10 mV voltage step to determine the capacitance, access, and input resistance. The access resistance varied from 1 to 6 MΩ and was compensated for. Experiments were excluded from analysis if the voltage errors originating from series resistance were >5 mV after compensation.

Data analysis

The holding potential was -80 mV, and the interpulse interval was at least 15 s unless noted otherwise. Details of voltage protocols (voltage range and step duration) were adjusted based upon the different biophysical properties of mutant channels. Time constants of activation, deactivation, onset, and recovery from inactivation were determined by fitting the current recordings with a single or double exponential function. The necessity of a second exponential component was judged both by inspection of difference plots and by F-statistics. Results are expressed as mean $\pm$ SE with n the number of cells analyzed. The relative contribution of each deactivation component (%) was calculated based upon the amplitudes of each component and normalized to the total amplitude. The voltage dependence of channel activation

was fitted with a Boltzmann equation: $y = 1/(1 + \exp[-(E - E_{1/2})/k])$, with E the applied voltage, $E_{1/2}$ the voltage at which 50% of the channels are activated, and k the slope factor. $1/k$ corresponds to zF/RT in which z is the equivalent charge and F, R, and T have their usual meanings. The voltage dependence of inactivation was determined as previously described (28). The Gibbs free energy of activation at 0 mV (ΔG_0) was calculated by $\Delta G_0 = 0.0002389 zFE_{1/2}$, with the factor 0.0002389 to express the values in Kcal/mol (29). The relationship between $E_{1/2}$ or ΔG_0 values and the local net charge of the KIKER sequence was fitted with a linear function. The time constants of the late phase of activation were fitted with a single exponential function. Their voltage dependence was fit with an exponential function, of which the baseline represents the saturating ('asymptotic') value of the activation time constant at strong depolarizations. Goodness-of-fit values r^2 and degree of freedom adjusted r^2 (DF adj. r^2) were calculated to assess the quality of all fitted functions. When needed, a Student's t-test for independent samples was used for statistical significance testing. A Mann Whitney U Rank Sum test was used when unequal variances between the data sets were present. The differences were accepted as significant for the tested p-value below 0.05.

RESULTS

The local electric field influences the voltage dependence of activation

N-terminal deletions in the proximal domain (amino acids 139–377 between the PAS domain and the S1 segment) have been shown to shift the voltage dependence of activation toward negative potentials independently from the inactivation process (16). Because this proximal domain contains multiple charged residues and since electrostatic interactions can easily alter the voltage dependence of activation, we investigated the involvement of a basic residue cluster in the last 19 amino acids of this domain in modulating the activation of HERG (Fig. 1). Therefore, we deleted almost the entire proximal domain (Δ143–372), whereas the remaining sections preceding and following the deletion site were left unchanged (Fig. 1). Compared to WT a large hyperpolarizing shift (~−50 mV) of the midpoint of activation was observed (Fig. 2; Table 1).

Since the WT proximal domain contains several charges close to the S1 segment, a subtotal deletion was created ranging from residues 171 to 372. This deletion (Δ171–372) was specifically designed to maintain a cluster of basic residues, mimicking the original charge distribution proximal to S1, as the C-end of the remaining sequence preceding the deletion contained several positively charged residues (Fig. 1). Although this subtotal deletion removed ~200 of the 240 amino acids of the proximal domain, the midpoint of activation was not significantly different from WT (Fig. 2;

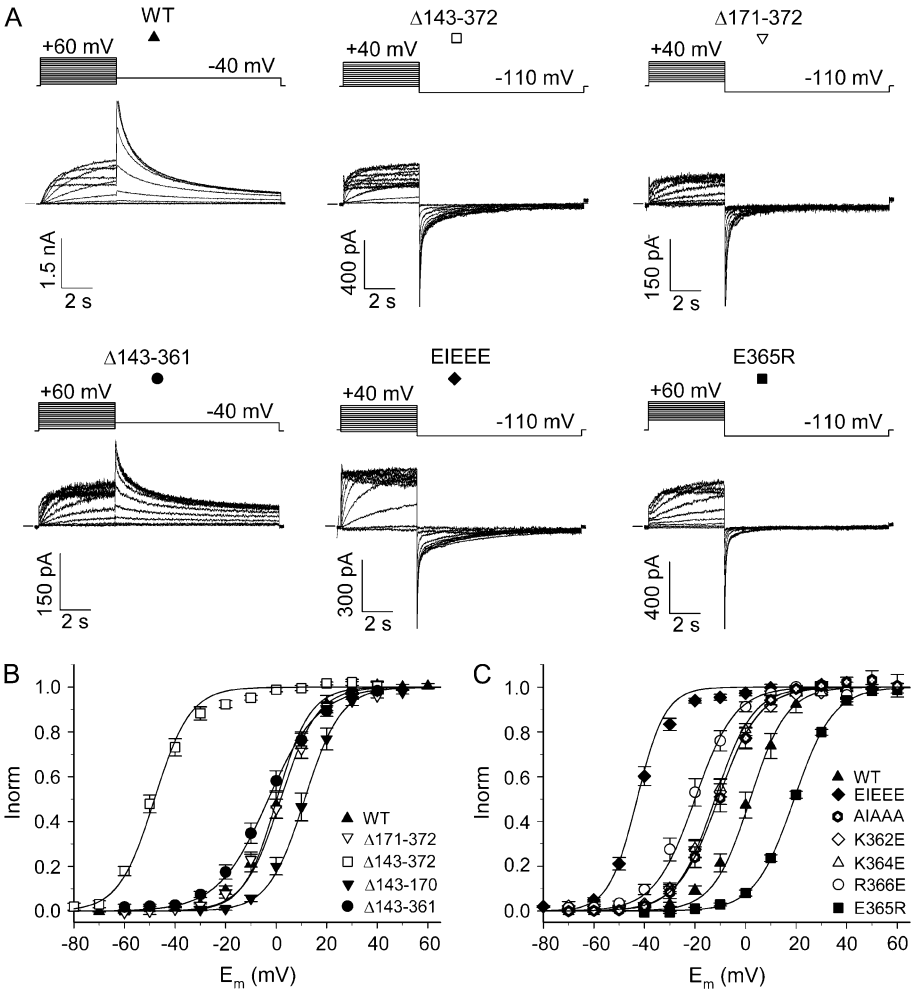

FIGURE 2 Voltage dependence of activation. (*A*) Raw current traces of WT HERG and of several deletion and charge reversal mutations with the applied voltage protocol on top. (*B*) Voltage dependence of activation of the deletion mutations compared to WT. Note the strong negative shift of the midpoint of activation for Δ143–372. (*C*) Voltage dependence of activation of charge reversal mutations compared to WT.

TABLE 1 Overview of the biophysical parameters for the different mutations analyzed

Construct	Sequence	Net charge	$E_{1/2}$ (mV)	k (mV)	ΔG_0 (Kcal/mol)	n
WT	K I K E R	+2	1.8 ± 1.8	7.3 ± 0.2	0.13 ± 0.1	14
Δ171-372		N.A.	0.3 ± 1.5	7.8 ± 0.3	0.02 ± 0.1	20
Δ143-372		N.A.	−48.1 ± 1.4*	7.8 ± 0.6	−3.37 ± 0.3	18
Δ143-170		N.A.	11.3 ± 1.6*	7.2 ± 0.2	0.86 ± 0.1	6
Δ143-361		N.A.	−3.1 ± 2.0	10.2 ± 0.5*	−0.17 ± 0.1	11
EIEEE	E I E E E	−4	−42.9 ± 0.9*	5.9 ± 0.4*	−3.96 ± 0.3	17
AIAAA	A I A A A		−10.8 ± 2.1*	8.1 ± 0.2*	−0.73 ± 0.1	5
K362E	E I K E R	0	−10.8 ± 1.9*	8.3 ± 0.4*	−0.71 ± 0.1	9
K364E	K I E E R	0	−12.1 ± 1.5*	7.6 ± 0.2	−0.87 ± 0.1	11
R366E	K I K E E	0	−20.0 ± 2.1*	8.1 ± 0.3*	−1.35 ± 0.2	12
E365R	K I K R R	+4	18.8 ± 0.6*	7.7 ± 0.2	1.33 ± 0.1	7

The local net charge, activation midpoint ($E_{1/2}$), slope factor (k), Gibbs free energy (ΔG_0) and n the number of cells analyzed are represented for each mutation.

*$p < 0.05$ compared to WT; N.A. not applicable.

Table 1). When this cluster of basic residues was also removed by deletion of an extra 30 amino acids (Δ143–372), a large negative shift was observed in the voltage dependence of activation (Fig. 2). Comparison of the N-terminal sequences in both constructs (i.e., Δ171–372 and Δ143–372) revealed that the net charge immediately preceding the respective deletion sites was opposite (Fig. 1). Hence, the observed difference in the voltage dependence of activation for both deletions suggests the involvement of the local charge distribution of the proximal domain in modulating the voltage dependence.

To test further whether the shift was not merely caused by the deletion of another 30 amino acids but by the alteration of the local charge distribution, two additional deletion mutations (Δ143–170 and Δ143–361) were created (Fig. 1). The Δ143–170 deletion displayed a mild depolarizing shift (~10 mV) compared to WT, implying that the profound hyperpolarizing shift in voltage dependence of activation of the Δ143–372 deletion compared to the Δ171–372 was not the result of having deleted these extra 30 amino acids (Fig. 2 *B*). The Δ143–361 deletion, removing almost the entire proximal domain while preserving the charges at the C-terminal part of the proximal domain, revealed a midpoint of activation comparable to that of WT (Fig. 2). Together, these results strongly suggest that the presence of charges in the C-terminal end (362–372) of the domain proximal to S1 is required to maintain a WT voltage dependence of activation and that alteration of the local charge distribution modulates the gating properties of HERG.

To investigate this further, we focused on the cluster of basic residues within the region of the terminal 11 residues of the proximal domain. The positively charged residues (K362, K364, R366) of the KIKER sequence were substituted by glutamate resulting in an EIEEE sequence (Fig. 1). In this case the midpoint of activation showed a hyperpolarizing shift of ~−45 mV, combined with a steepening of the slope factor when compared to WT (Fig. 2, Table 1). The magnitude of the hyperpolarizing shift induced by the EIEEE mutation was similar to the one induced by the near total proximal domain deletion (Δ143–372). Substitution of all charged residues by alanine (i.e., AIAAA) shifted the midpoint of activation by ~−12 mV (Table 1).

To assess the relative contribution of each charge, the basic residues were each substituted individually by a negatively charged glutamate (Fig. 1). Each substitution consistently displayed a negative shift in the voltage dependence of activation that was intermediate to WT and the triple mutant (EIEEE). The shift of the R366E mutation was more pronounced compared to that of the K362E and K364E mutations (Fig. 2; Table 1). Conversely, changing the glutamate of the KIKER sequence to arginine (E365R) shifted the voltage dependence of activation by ~20 mV to more positive potentials (Fig. 2; Table 1).

To evaluate whether the effects on the voltage dependence of activation correlate with the net charge of the KIKER sequence, the midpoint of activation was plotted as a function of the net charges of the different mutants (Fig. 3). A linear function provided a good fit indicating that the $E_{1/2}$-values correlate well with the local net charge of the KIKER region. When the altered voltage dependence is expressed in terms of Gibbs free energy (30–32), a similar linear correlation was observed for a local net charge ranging from −4 to +4 (Supplemental Fig. S1). Both approaches indicate that the charges within this segment contribute in an additive manner to the observed effects.

Forward rate constants of early opening transitions are enhanced by negative charges at the end of the proximal domain

The 'three-closed-state' activation model ($C_0 \leftrightarrow C_1 \leftrightarrow C_2 \leftrightarrow O \leftrightarrow I$) described by Wang et al. (33) included a weakly voltage-dependent activation step ($C_0 \rightarrow C_1$), necessary to describe the activation behavior of HERG adequately. In this model, the authors described that the initial sigmoidal delay in the activating current largely reflected the early $C_0 \rightarrow C_1$ state transition (33,34), although not exclusively since HERG gating comprises a multistep process. Consequently, an estimate

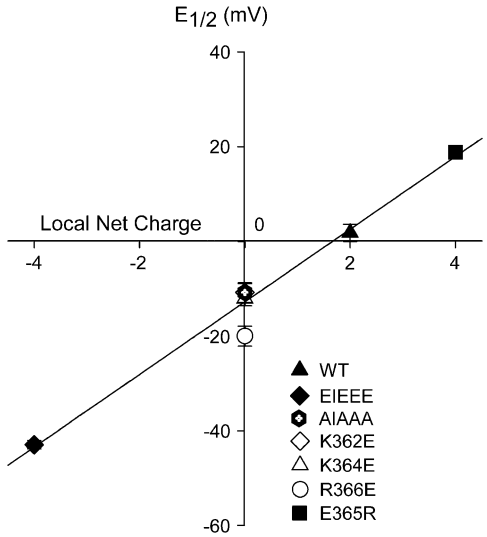

FIGURE 3 Correlation between the midpoint of activation and the local net charge of the KIKER sequence. $E_{1/2}$-values were plotted as a function of the local net charge for WT, for the charge reversal mutants (i.e., EIEEE, K362E, K364E, R366E, E365R) and for the AIAAA mutant (Fig. 1). The solid line represents the linear function that was fitted to the data. Goodness-of-fit values were $r^2 = 0.99$ and DF adj. $r^2 = 0.99$ (see Materials and Methods).

of the $C_0 \rightarrow C_1$ rate constant is obtained by quantifying the sigmoidal delay of activation. Therefore, we determined the time lag between the start of the voltage step and the zero-current time point extrapolated from the exponential rising phase, as illustrated in Fig. 4. It showed that WT, the Δ171–372, and the EIEEE mutations displayed a pronounced delay and sigmoidal phase, whereas the delay was nearly absent in the Δ143–372 mutation. Evaluation of the time lag values confirmed this with values of 53 ± 8 ms and 47 ± 18 ms for WT and the Δ171–372 mutation, respectively. In contrast, the time lag was 8 ± 3 ms for the near total deletion Δ143–372, whereas an intermediate value of 34 ± 6 ms was observed for the charge reversal mutant (EIEEE) (Fig. 4). These data indicate that charge reversal by deletion (Δ143–372) causes faster forward $C_0 \rightarrow C_1$ opening rates, whereas the EIEEE only shows a modest tendency toward an accelerated early opening transition.

In contrast to the first $C_0 \rightarrow C_1$ transition, the intermediate $C_1 \rightarrow C_2$ opening transition in this model is largely voltage independent and becomes dominant during the late phase of the activation at more positive potentials. This is reflected by the saturation of the rate of activation as the depolarization further increases. Consequently, the $C_1 \rightarrow C_2$ rate can be estimated by the saturating value of the activation time constant at strong depolarization (33). To obtain these asymptotic time constants and to overcome confounding effects of rapid inactivation during channel opening, a pulse protocol was used as shown in Fig. 5 (33,35). The asymptotic values were faster for both the Δ143–372 and the EIEEE mutations (133 ± 17, 93 ± 5 ms) compared to WT (181 ± 21 ms), indicating that charge reversal at the end of the proximal domain accelerated the voltage-independent $C_1 \rightarrow C_2$ transition but with a more pronounced effect for the EIEEE mutation compared to the deletion mutant (Fig. 5).

Relation between gating kinetics and the steady-state voltage dependence of activation

The time constants of activation for the Δ143–372 mutation were faster in comparison with WT, whereas the other deletion mutations (Δ171–372, Δ143–170, and Δ143–361) showed

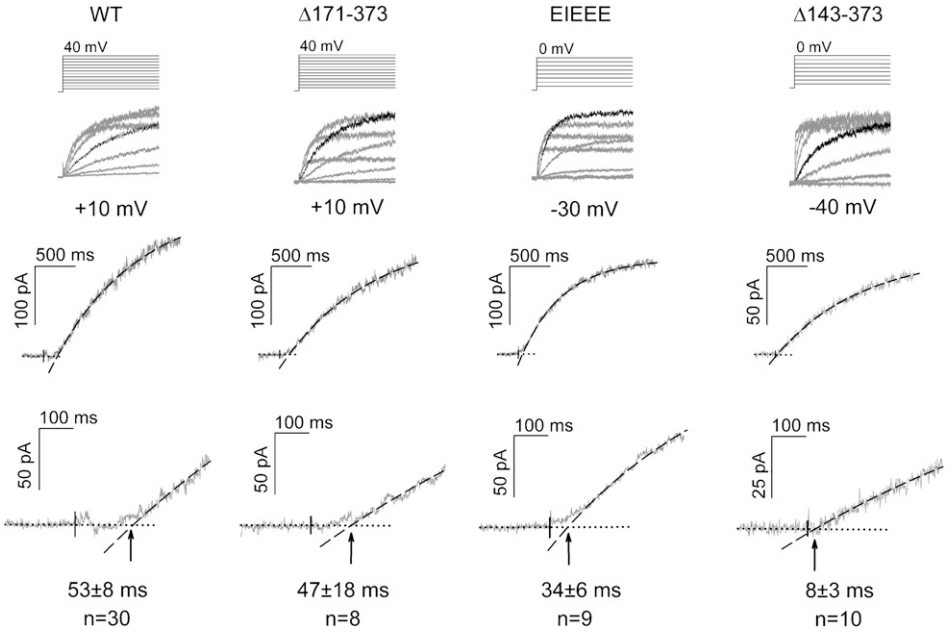

FIGURE 4 Estimation of the early forward rate constant during channel activation. (*Top*) Voltage protocols that were used to induce channel activation. Underneath in gray are the leak-corrected raw current traces of WT and the constructs Δ171–372, EIEEE, and Δ143–372. For each construct the current trace corresponding to the potential analyzed is highlighted in black (+10 mV for WT and Δ171–372; −30 mV for EIEEE and −40 mV for Δ143–372). These potentials were chosen to account for the respective shifts of voltage dependence of activation. (*Middle*) Enhanced view of the current traces analyzed. The dotted line corresponds to zero current, and the dashed line corresponds to the exponential fit and the extrapolation. (*Bottom*) Expanded view of these current traces. Note the shortening of the time lag (*arrows*) for the EIEEE construct and especially the Δ143–372 mutation. The values of the time lag are given below the tracings.

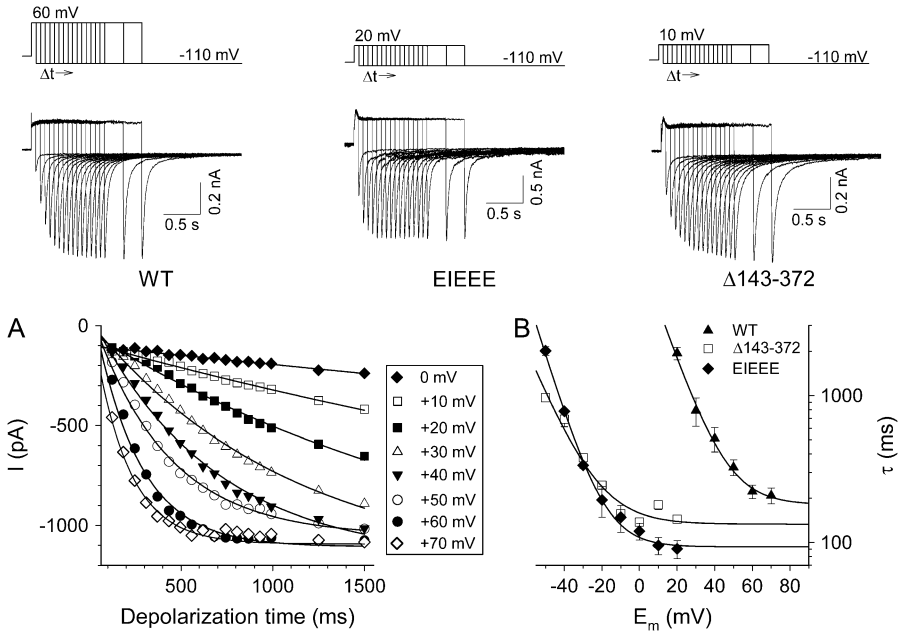

FIGURE 5 Estimation of the intermediate forward rate constant during channel activation. (*Top*) Pulse protocols that were used for the assessment of the time course of HERG activation. Representative currents were elicited by repolarization to −110 mV after depolarizations to +60, +20, and +10 mV for WT, EIEEE, and Δ143–372 channels, respectively, while varying the step duration. (*A*) Time course of activation of WT HERG at different voltages. Peak tail currents were plotted against the applied depolarization time for each voltage step. Solid lines represent the single exponentials that were fitted to obtain the late phase of the activation time constants. (*B*) Voltage dependence of the activation time constants. The time constants of the late phase activation were plotted as a function of the applied voltage. The solid line represents a single exponential fit to the time constants. The asymptotic values were derived from these fits.

activation time constants similar to WT. The deactivation of all deletion mutations was comparable to WT (Fig. 6 *A*).

At first glance, the replacement of the positively charged residues in the KIKER sequence by negative glutamate residues showed a faster activation that was most pronounced for the EIEEE mutation and intermediate for the individual charge reversal mutations (Fig. 6, *B* and *C*). When an additional positive charge was introduced, resulting in the sequence KIKRR (Fig. 1), a slowing of the activation kinetics was observed (Fig. 6 *C*). The introduction of negative charges in the KIKER sequence caused only minor changes in the fast and slow components of the deactivation kinetics (Fig. 6).

However, to account for the large shifts of the midpoint of activation described above, the time constants were plotted after correction for the shift in voltage dependence of activation (Fig. 7). The normalized kinetic data showed no significant differences in the activation time constants for most mutations compared to WT except for the EIEEE mutation, which was slightly faster (Fig. 7 *A*). However, in contrast to the activation kinetics, the deactivation time constants were noticeably faster for the Δ143–372 and EIEEE mutations but remained unaltered for all other mutations compared to WT (Fig. 7). The relative contribution of both fast and slow deactivation components was similar for all mutations analyzed (Fig. 7 *D*). Thus, when the respective shifts of voltage dependence of activation were taken into account, an acceleration of the deactivation was only observed when the local charge became more negative.

Assessment of the inactivation kinetics and of the voltage dependence of inactivation revealed only minor differences for all mutants (Fig. 8). The isochronal IV relationship is presented in panel *B* of Fig. 8 and shows that the overall shape remained the same, with a shift along the voltage axis reflecting the shifts in $E_{1/2}$.

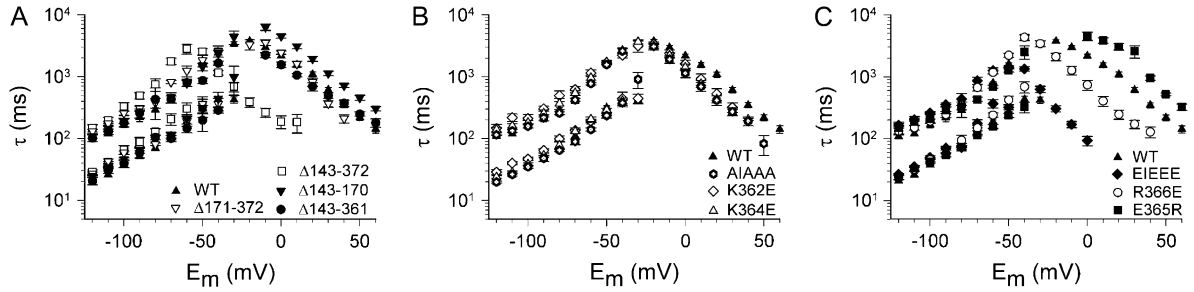

FIGURE 6 Voltage dependence of activation and deactivation kinetics. (*A*) The Δ171–372 mutant behaved similarly to WT for both activation and deactivation, but for the Δ143–372 deletion a 10-fold acceleration of the activation was observed with minor effects on deactivation. (*B*) Kinetics for charge reversal mutations was similar to WT for the deactivation, whereas the time constants of activation were faster for the EIEEE mutation compared to WT. Conversely, an additional positive charge (E365R) resulted in slowing of the activation time constants. (*C*) Deactivation kinetics was similar to WT for all charge reversals; significant differences in the activation kinetics were observed for E365R (slower) and EIEEE (faster).

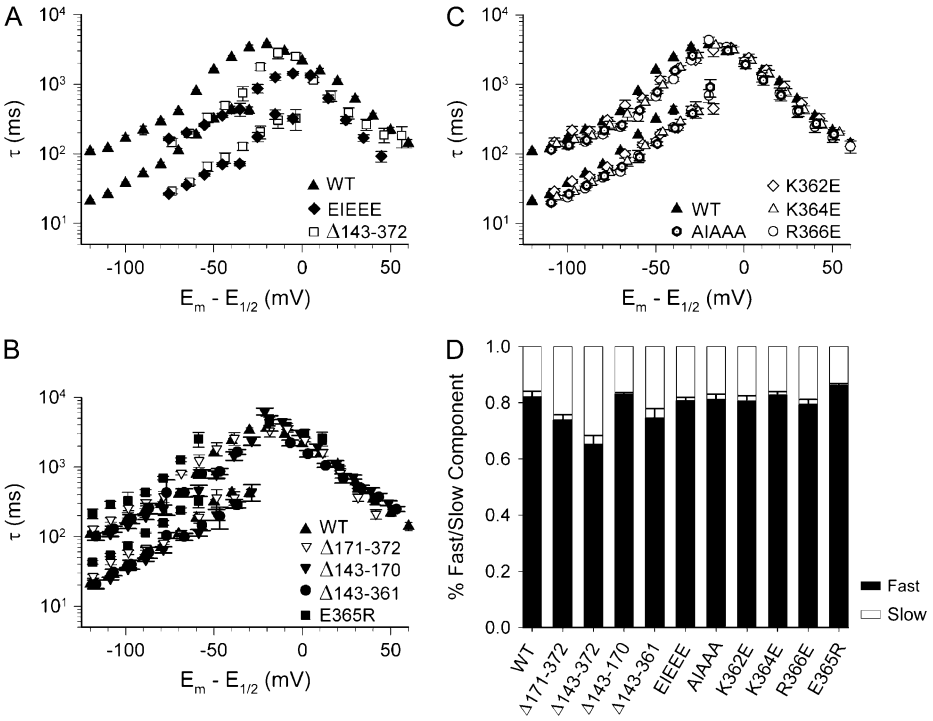

FIGURE 7 Kinetics of deactivation and activation normalized to the shifts in the voltage dependence of activation. The time constants (as in Fig. 6) were shifted along the voltage axis according to the midpoint of activation. (*A*) The differences in the voltage dependence of the activation kinetics (Fig. 6, *A–C*) largely disappeared after the correction for the differences in $E_{1/2}$. However, for the EIEEE and the Δ143–372 deletion an acceleration of deactivation is evident after this adjustment. (*B*) Introduction of positive charges induced minor effects on deactivation kinetics for E365R, whereas the deletion mutations (Δ171–372, Δ143–170, Δ143–361) were similar to WT. The activation time constants were comparable to WT for all mutations. (*C*) The neutral AIAAA mutant and the mutations with a single substitution by a negative charge all showed minor acceleration of deactivation but no effect on activation. (*D*) Relative contribution (amplitude) of the fast and slow components of the deactivation (%) derived from double exponential fits. The contribution of the fast component is shown in black; the slow component is shown in gray. The fast component was predominant (65–85%) in all cases.

DISCUSSION

The charges of the KIKER sequence modulate the gating properties

The intracellular N-terminus has been shown to modulate the gating properties of voltage-gated potassium channels. Several studies have addressed the structure-function relation of the PAS domain and its interaction with the gating machinery of HERG channels (14,16–18,22,23,25,26). Deletions (partial or complete) within the proximal domain also alter gating properties as evidenced by large hyperpolarizing shifts in the voltage dependence of activation (16), similar to the effect of the near total deletion (Δ143–372) reported here. These deletions change the charge distribution in the remaining section immediately in front of S1 as the cluster of basic residues (KIKER) is replaced by acidic residues. Deletion of ~220 amino acids, preserving a cluster of mainly positively charged residues upstream to S1 (Δ143–361), displayed activation properties that closely resembled WT. These results indicate that a large part of the proximal domain is not essential for a WT HERG activation phenotype.

Substitution of each positive residue of the KIKER sequence by a negative one consistently resulted in a negative shift of the voltage dependence of activation of varying magnitude (R366E > K364E ≈ K362E). When all three basic residues were substituted (EIEEE), the hyperpolarizing shift was similar to that of the near total proximal domain deletion (Δ143–372). In contrast, exchanging the negative charge E365 to an arginine shifted the midpoint of activation to more depolarized potentials. These results indicate that the modulatory effect of the proximal domain can largely be attributed to the charged cluster of the KIKER region. The negative shift of the activation curve with the EIEEE mutation indicates that the closed state is destabilized compared to WT.

The proximal domain influences the rates of the early opening transitions

For HERG a 'three-closed-state' activation model has been proposed with two voltage-sensitive and one intermediate voltage-insensitive transition (33,34,36). In this context it was shown that deletion of the proximal domain primarily accelerated the voltage-sensitive $C_0 \rightarrow C_1$ and the intermediate voltage-insensitive $C_1 \rightarrow C_2$ transitions (16).

To evaluate whether both the EIEEE mutation and the Δ143–372 deletion alter the first two opening transitions ($C_0 \rightarrow C_1$ and $C_1 \rightarrow C_2$) differently, the forward rate constants of both opening transitions were estimated (33). Based on the sigmoidal delay in activation, the Δ143–372 deletion accelerated the $C_0 \rightarrow C_1$ transition almost sevenfold, whereas the EIEEE charge reversal caused only a modest increase in the $C_0 \rightarrow C_1$ rates. Since inactivation is fast, changes in inactivation kinetics might alter the sigmoidal delay in activation. The inactivation time constants for the Δ143–372 deletion (at −40 mV) and the EIEEE mutation (at −30 mV) were comparable to WT (at +10 mV). Also, the voltage dependence of inactivation was similar for all constructs. Hence the inactivation process could not explain the fourfold difference of the sigmoidal delay between the Δ143–372 deletion and the EIEEE mutation. We conclude that the observed differences

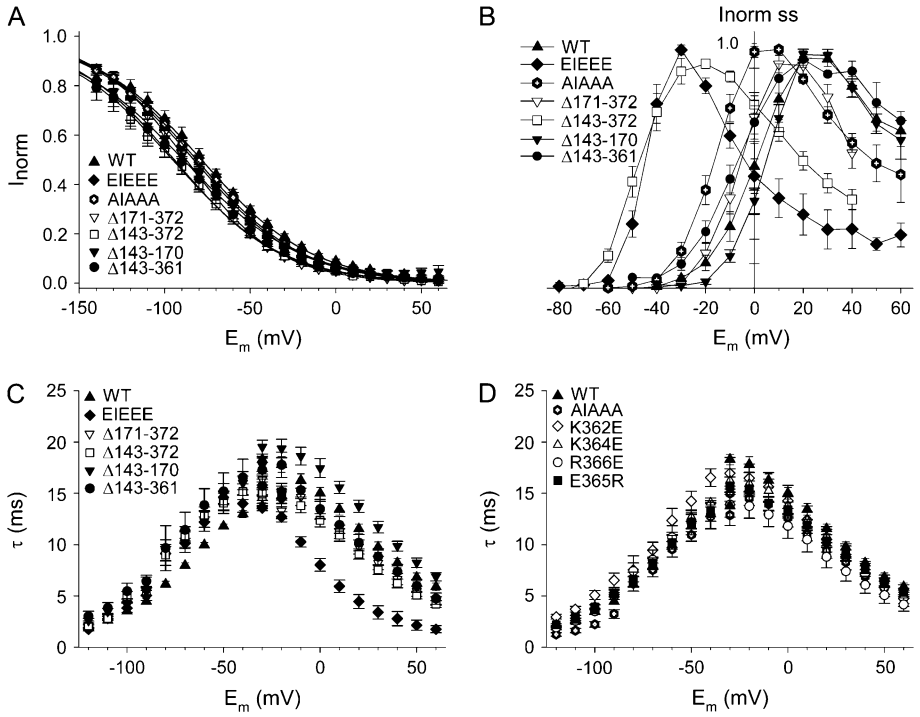

FIGURE 8 Voltage dependence and kinetics of inactivation. (*A*) The voltage dependence of inactivation was comparable for all mutations analyzed. (For protocol see Materials and Methods section) (*B*) Current-voltage relationship for the steady-state current as a function of voltage, normalized to the maximal current for each mutation. (*C*) The kinetics of onset and recovery of inactivation displayed faster time constants of inactivation for the EIEEE between −20 mV and +60 mV, whereas the time constants for the deletion mutations resemble those of WT. (*D*) Time constants of recovery and onset of inactivation of the charge reversal mutations were comparable to those of WT.

in sigmoidal delay are primarily caused by alterations in the early $C_0 \rightarrow C_1$ rates.

The asymptotic values of the activation time constants indicate that the $C_1 \rightarrow C_2$ rates are faster for the EIEEE and the Δ143–372 deletion compared to WT, with EIEEE showing the most pronounced effect. Overall, the charge reversal in a full length N-terminus (EIEEE) primarily affected the intermediate voltage-independent $C_1 \rightarrow C_2$ transition, whereas deletion of the proximal domain (Δ143–372) induced an additional acceleration of the $C_0 \rightarrow C_1$ transition, consistent with previous reports (16,27). Simulation of the 'three-closed-state' model largely reproduced the effects on the voltage dependence of activation and were in agreement with the experimental data presented here (Fig. S2). In summary, the charges of the KIKER sequence influence the voltage dependence of activation predominantly by altering the intermediate opening transition $C_1 \rightarrow C_2$. The apparent speeding of this voltage-independent $C_1 \rightarrow C_2$ transition may account for the observed steepening of the slope factor in conjunction with the negatively shifted $E_{1/2}$, a correlation that was already described for *Shaker*-type K channels (37). Conversely, it is possible that the additional acceleration of the $C_0 \rightarrow C_1$ transition (Δ143–372) is reflected in the combination of a shallow slope with a negative shift. These data indicate that although the negative shift in voltage dependence of activation was of a similar magnitude for both mutations (EIEEE and Δ143–372), the mechanisms causing the shifts were not entirely identical. The near total deletion of the proximal domain probably disturbs the conformation of the N-terminus and the way it interacts with other regions of the channel. Hence, it is tempting to speculate that although the net local charge proximal to S1 is comparable for the EIEEE mutation and the Δ143–372 deletion, the interaction with the channel core need not be.

The gating properties are altered through electrostatic interaction but not through alteration of the surface charge

Our data clearly show that the magnitude of the shifts of voltage dependence of activation, expressed as activation midpoint or ΔG_0, was strongly dependent on the net charge of the KIKER mutations (Figs. 3 and S1). Admittedly, the Gibbs free energy analysis is based upon the assumption of a two-state gating model which does not really apply to the 'three-closed-state' gating model of HERG. However, the activation curves could be fitted appropriately with a single Boltzmann function (see also (30–32)). Furthermore, the ΔG_0 approach takes into account both the midpoint of activation and the slope factor. In this perspective, the additive contribution of each charged residue (ranging from −4 to +4) is indicative of electrostatic interactions. Consequently, the potential interaction site(s) near the channel core are most likely charged clusters, although we cannot fully exclude a multipoint interaction with other charged regions within the N-terminus (25).

If the KIKER sequence directly affects the local electrical field sensed by the S4 voltage sensor (surface charge effect), then substituting the positively charged cluster by a negative one (EIEEE instead of KIKER) would be expected to induce a shift in the positive direction. However the opposite effect

was observed, making a pure surface charge effect on the S4 charges unlikely, indicating that the effect involves interaction with other structures important for gating.

During the process of gate opening, the voltage sensor reorients before the actual gating charges are moved and gating currents can be measured (38,39). Because the distal charges of S4 do not seem to participate in the actual voltage sensing, it is possible that the bottom part of the S4 segment may be involved in this early reorientation of the voltage sensor (32). However, if the charged residues of the KIKER sequence interact with these charges at the bottom of S4, one would expect a stabilizing effect of introducing negative charges, opposite to what was observed (Fig. 2). Alternatively, depending on the position of the KIKER region relative to the bottom of the S4, a more elaborate speculation would be that the native positive charges restrain the early reorientation, in which case introduction of negative charges might remove such electrostatic constraint.

Such an electrostatic restraint does not need to be limited to the bottom part of S4 and may include other regions (i.e., S4-S5 linker, bottom of S6) involved in coupling the process of voltage sensing to gate opening and closure. In this context, Sanguinetti and co-workers have established that electrostatic interactions are an important part of the gating process (40–42). It is therefore conceivable that charged regions in other parts of the channel, such as the N-terminal KIKER sequence, modify the gating process. Since the interaction of D540 (S4-S5 linker) with R665 (S6) may stabilize the closed state, one could speculate that introducing more negative charges would destabilize this interaction, and hence the closed state (40).

Activation and deactivation kinetics

The speed at which the activating and deactivating state transitions occur is determined by the rate-limiting steps of the gating process. This is a dynamic event with sequential movement of the voltage sensor that becomes translated into movements of the activation gate, opening or closing the permeation pathway (39). Hence, it is conceivable that activation and deactivation rates are determined by the underlying structure of the gate and of other regions that constitute the gating machinery rather than the movements of the voltage sensor. As the KIKER sequence predominantly influences the voltage dependence of activation upon charge reversal, the corresponding shifts have to be taken into account when interpreting the activation kinetics. Since the corrected activation rates did not reveal large differences (Fig. 7), likely only minor changes occur at the gating machinery during opening when charges of the KIKER sequence are substituted.

More caution should be exercised when interpreting the deactivation kinetics. Since the mechanism of deactivation is not fully understood, it is an open question to what extent the gate region remains coupled to the voltage sensor movements upon channel closure (43).

If channel closure is indirectly coupled to the voltage sensor movements, the time constants of deactivation do not have to be corrected for the corresponding shifts in voltage dependence of activation. In that case, the mutations of the KIKER sequence do not influence deactivation (Fig. 6).

On the other hand, if coupling exists during the entire gating process (42,43), then the voltage dependence of activation must be taken into account to assess the deactivation rates. Consequently faster closure rates are observed as the charges in the proximal domain become more negative (Fig. 7). This is opposite to what is expected based on a mechanistic coupling between voltage sensor and gate movement. This would imply that the interaction between the proximal domain and the channel core is a dynamic process that may involve multipoint interactions that include other regions important for channel closure.

A prime candidate would be the PAS domain, because similar accelerations of the deactivation kinetics were observed by deletions or mutations of the PAS domain (14,22,23) and of the first 16 N-terminal amino acids (24–26). It is possible that charges throughout the N-terminus play a role in orienting the PAS domain toward its yet unknown site of interaction. This could explain the similarities of the deactivation kinetics observed between mutations in the PAS domain and mutations elsewhere in the N-terminus. Alternatively, the KIKER sequence may also have a distinct role in the modulation of channel opening since the effects on the voltage dependence of activation shown here were not observed with mutations of other N-terminal regions. These data strengthen the idea that the amino terminus plays an important role in channel gating through dynamic multisite interaction.

In conclusion, our study demonstrates that a small cluster of basic residues within the N-terminus affects the activation process of HERG, whereas almost 220 amino acids of the proximal domain are apparently not essential for a normal activation phenotype. The results suggest that the local electric field of a small section within the proximal domain close to the S1 segment is important for the modulatory effects on channel gating. Although further investigation is needed to elucidate the exact regions of interaction involved, we propose electrostatic interactions on the gating machinery as the main mechanism.

SUPPLEMENTARY MATERIAL

An online supplement to this article can be found by visiting BJ Online at http://www.biophysj.org.

We thank Tessa de Block for her excellent technical assistance. J.B.S. and A.J.L. are doctoral and postdoctoral fellows, respectively, with the ''Fonds voor Wetenschappelijk Onderzoek Vlaanderen'' (FWO).

This work was supported by grants from the Flanders Institute for Biotechnology (VIB PRJ05) and the ''Fonds voor Wetenschappelijk Onderzoek Vlaanderen'' (FWO-G0152.06, FWO-1.5.047.05).

REFERENCES

1. Mitcheson, J. S., and M. C. Sanguinetti. 1999. Biophysical properties and molecular basis of cardiac rapid and slow delayed rectifier potassium channels. *Cell. Physiol. Biochem.* 9:201–216.
2. Zhou, Z., Q. Gong, B. Ye, Z. Fan, J. C. Makielski, G. A. Robertson, and C. T. January. 1998. Properties of HERG channels stably expressed in HEK 293 cells studied at physiological temperature. *Biophys. J.* 74:230–241.
3. Spector, P. S., M. E. Curran, A. Zou, M. T. Keating, and M. C. Sanguinetti. 1996. Fast inactivation causes rectification of the I_{Kr} channel. *J. Gen. Physiol.* 107:611–619.
4. Sanguinetti, M. C., C. Jiang, M. E. Curran, and M. T. Keating. 1995. A mechanistic link between an inherited and an acquired cardiac arrhythmia: HERG encodes the I_{Kr} potassium channel. *Cell.* 81: 299–307.
5. Curran, M. E., I. Splawski, K. W. Timothy, G. M. Vincent, E. D. Green, and M. T. Keating. 1995. A molecular basis for cardiac arrhythmia: HERG mutations cause long QT syndrome. *Cell.* 80:795–803.
6. Roden, D. M. 2006. Long QT syndrome: reduced repolarization reserve and the genetic link. *J. Intern. Med.* 259:59–69.
7. Doyle, D. A., J. M. Cabral, R. A. Pfuetzner, A. Kuo, J. M. Gulbis, S. L. Cohen, B. T. Chait, and R. MacKinnon. 1998. The structure of the potassium channel: molecular basis of K^+ conduction and selectivity. *Science.* 280:69–77.
8. Jiang, Y., A. Lee, J. Chen, V. Ruta, M. Cadene, B. T. Chait, and R. MacKinnon. 2003. X-ray structure of a voltage-dependent K^+ channel. *Nature.* 423:33–41.
9. Long, S. B., E. B. Campbell, and R. MacKinnon. 2005. Crystal structure of a mammalian voltage-dependent Shaker family K+ channel. *Science.* 309:897–903.
10. Bezanilla, F. 2000. The voltage sensor in voltage-dependent ion channels. *Physiol. Rev.* 80:555–592.
11. Long, S. B., E. B. Campbell, and R. MacKinnon. 2005. Voltage sensor of Kv1.2: structural basis of electromechanical coupling. *Science.* 309:903–908.
12. Aggarwal, S. K., and R. MacKinnon. 1996. Contribution of the S4 segment to gating charge in the Shaker K^+ channel. *Neuron.* 16:1169–1177.
13. Seoh, S. A., D. Sigg, D. M. Papazian, and F. Bezanilla. 1996. Voltage-sensing residues in the S2 and S4 segments of the Shaker K^+ channel. *Neuron.* 16:1159–1167.
14. Morais Cabral, J. H., A. Lee, S. L. Cohen, B. T. Chait, M. Li, and R. MacKinnon. 1998. Crystal structure and functional analysis of the HERG potassium channel N terminus: a eukaryotic PAS domain. *Cell.* 95:649–655.
15. Warmke, J. W., and B. Ganetzky. 1994. A family of potassium channel genes related to eag in Drosophila and mammals. *Proc. Natl. Acad. Sci. USA.* 91:3438–3442.
16. Viloria, C. G., F. Barros, T. Giraldez, D. Gomez-Varela, and P. de la Pena. 2000. Differential effects of amino-terminal distal and proximal domains in the regulation of human erg K(+) channel gating. *Biophys. J.* 79:231–246.
17. Paulussen, A., A. Raes, G. Matthijs, D. J. Snyders, N. Cohen, and J. Aerssens. 2002. A novel mutation (T65P) in the PAS domain of the human potassium channel HERG results in the long QT syndrome by trafficking deficiency. *J. Biol. Chem.* 277:48610–48616.
18. Rossenbacker, T., K. Mubagwa, R. J. Jongbloed, J. Vereecke, K. Devriendt, M. Gewillig, E. Carmeliet, D. Collen, H. Heidbuchel, and P. Carmeliet. 2005. Novel mutation in the Per-Arnt-Sim domain of KCNH2 causes a malignant form of long-QT syndrome. *Circulation.* 111:961–968.
19. Splawski, I., J. Shen, K. W. Timothy, G. M. Vincent, M. H. Lehmann, and M. T. Keating. 1998. Genomic structure of three long QT syndrome genes: KVLQT1, HERG, and KCNE1. *Genomics.* 51: 86–97.
20. London, B., M. C. Trudeau, K. P. Newton, A. K. Beyer, N. G. Copeland, D. J. Gilbert, N. A. Jenkins, C. A. Satler, and G. A. Robertson. 1997. Two isoforms of the mouse ether-a-go-go-related gene coassemble to form channels with properties similar to the rapidly activating component of the cardiac delayed rectifier K^+ current. *Circ. Res.* 81:870–878.
21. Jones, E. M., E. C. Roti Roti, J. Wang, S. A. Delfosse, and G. A. Robertson. 2004. Cardiac IKr channels minimally comprise hERG 1a and 1b subunits. *J. Biol. Chem.* 279:44690–44694.
22. Chen, J., A. Zou, I. Splawski, M. T. Keating, and M. C. Sanguinetti. 1999. Long QT syndrome-associated mutations in the Per-Arnt-Sim (PAS) domain of HERG potassium channels accelerate channel deactivation. *J. Biol. Chem.* 274:10113–10118.
23. Wang, J., M. C. Trudeau, A. M. Zappia, and G. A. Robertson. 1998. Regulation of deactivation by an amino terminal domain in human ether-a-go-go-related gene potassium channels. *J. Gen. Physiol.* 112: 637–647.
24. Terlau, H., S. H. Heinemann, W. Stuhmer, O. Pongs, and J. Ludwig. 1997. Amino terminal-dependent gating of the potassium channel rat eag is compensated by a mutation in the s4 segment. *J. Physiol. (Lond.).* 502:537–543.
25. Wang, J., C. D. Myers, and G. A. Robertson. 2000. Dynamic control of deactivation gating by a soluble amino-terminal domain in HERG K(+) channels. *J. Gen. Physiol.* 115:749–758.
26. Schonherr, R., and S. H. Heinemann. 1996. Molecular determinants for activation and inactivation of HERG, a human inward rectifier potassium channel. *J. Physiol. (Lond.).* 493:635–642.
27. Gomez-Varela, D., P. de la Pena, J. Garcia, T. Giraldez, and F. Barros. 2002. Influence of amino-terminal structures on kinetic transitions between several closed and open states in human erg K^+ channels. *J. Membr. Biol.* 187:117–133.
28. Paulussen, A. D., A. Raes, R. J. Jongbloed, R. A. Gilissen, A. A. Wilde, D. J. Snyders, H. J. Smeets, and J. Aerssens. 2005. HERG mutation predicts short QT based on channel kinetics but causes long QT by heterotetrameric trafficking deficiency. *Cardiovasc. Res.* 67:467–475.
29. Li-Smerin, Y., D. H. Hackos, and K. J. Swartz. 2000. A localized interaction surface for voltage-sensing domains on the pore domain of a K^+ channel. *Neuron.* 25:411–423.
30. Subbiah, R. N., C. E. Clarke, D. J. Smith, J. Zhao, T. J. Campbell, and J. I. Vandenberg. 2004. Molecular basis of slow activation of the human ether-a-go-go related gene potassium channel. *J. Physiol.* 558: 417–431.
31. Subbiah, R. N., M. Kondo, T. J. Campbell, and J. I. Vandenberg. 2005. Tryptophan scanning mutagenesis of the HERG K+ channel: the S4 domain is loosely packed and likely to be lipid exposed. *J. Physiol.* 569:367–379.
32. Piper, D. R., W. A. Hinz, C. K. Tallurri, M. C. Sanguinetti, and M. Tristani-Firouzi. 2005. Regional specificity of human ether-a'-go-go-related gene channel activation and inactivation gating. *J. Biol. Chem.* 280:7206–7217.
33. Wang, S., S. Liu, M. J. Morales, H. C. Strauss, and R. L. Rasmusson. 1997. A quantitative analysis of the activation and inactivation kinetics of HERG expressed in Xenopus oocytes. *J. Physiol. (Lond.).* 502: 45–60.
34. Johnson, J. P. Jr., F. M. Mullins, and P. B. Bennett. 1999. Human ether-a-go-go-related gene K+ channel gating probed with extracellular CA2+. Evidence for two distinct voltage sensors. *J. Gen. Physiol.* 113:565–580.
35. Liu, S., R. L. Rasmusson, D. L. Campbell, S. Wang, H. C. Strauss, S. G. Liu, and S. M. Wang. 1996. Activation and inactivation kinetics of an E-4031-senstitive current from single ferret atrial myocytes. *Biophys. J.* 70:2704–2715.
36. Kiehn, J., A. E. Lacerda, and A. M. Brown. 1999. Pathways of HERG inactivation. *Am. J. Physiol.* 277:H199–H210.
37. Yifrach, O., and R. MacKinnon. 2002. Energetics of pore opening in a voltage-gated K(+) channel. *Cell.* 111:231–239.

38. Bannister, J. P., B. Chanda, F. Bezanilla, and D. M. Papazian. 2005. Optical detection of rate-determining ion-modulated conformational changes of the ether-a-go-go K+ channel voltage sensor. *Proc. Natl. Acad. Sci. USA.* 102:18718–18723.

39. Bezanilla, F. 2005. Voltage-gated ion channels. *IEEE Trans. Nanobioscience.* 4:34–48.

40. Tristani-Firouzi, M., J. Chen, and M. C. Sanguinetti. 2002. Interactions between S4–S5 linker and S6 transmembrane domain modulate gating of HERG K+ channels. *J. Biol. Chem.* 277:18994–19000.

41. Sanguinetti, M. C., and Q. P. Xu. 1999. Mutations of the S4–S5 linker alter activation properties of HERG potassium channels expressed in Xenopus oocytes. *J. Physiol.* 514:667–675.

42. Ferrer, T., J. Rupp, D. R. Piper, and M. Tristani-Firouzi. 2006. The S4–S5 linker directly couples voltage sensor movement to the activation gate in the human ether-a-go-go-related gene (hERG) K+ channel. *J. Biol. Chem.* 281:12858–12864.

43. Ding, S., and R. Horn. 2003. Effect of S6 tail mutations on charge movement in Shaker potassium channels. *Biophys. J.* 84:295–305.